[Review Paper]

Synthesis of Light Olefins from Oxygenated Organic Compounds over Metallosilicates with MFI and MTW-type Zeolite Structures

Yuta NAKASAKA [†1)]*, Teruoki TAGO [†2)], and Takao MASUDA [†1)]

[†1)] Div. of Applied Chemistry, Faculty of Engineering, Hokkaido University, N13 W8, Kita-ku, Sapporo 060-8628, JAPAN
[†2)] Dept. of Chemical Science and Engineering, School of Materials and Chemical Technology, Tokyo Institute of Technology, 2-12-1 Ookayama, Meguro-ku, Tokyo 152-8552, JAPAN

(Received May 9, 2017)

Selective production of light olefins over zeolite catalyst requires control of consecutive reactions because the objective products are intermediates. In catalytic reactions using zeolite, the diffusion resistance of both the raw material and products within the crystal, and acid site strength of the zeolite, strongly affect the catalyst activity and selectivity. This review describes the preparation of macro-, and nano-sized ferrisilicate and ferroaluminosilicate with MFI and MTW-type zeolite structures and their application to the production of light olefins from oxygenated organic compounds such as acetone and methanol. Nano-sized ferrisilicate with MFI-type zeolite structure showed more stable activity compared to macro-sized zeolite in the acetone to olefin and methanol to olefin reactions. Moreover, metallosilicates containing Fe atoms in the zeolite framework had higher selectivity for light olefins compared to aluminosilicate due to suppression of the consecutive reactions forming aromatics and coke. Ferroaluminosilicate containing two types of Brønsted acid sites, derived from both Fe and Al atoms in the framework, was the most effective catalyst for the production of light olefins from methanol.

Keywords
Light olefin, Metallosilicate, Crystal size, Acid site strength, Oxygenated organic compound

1. Introduction

Light olefins such as ethylene, propylene and butenes are essential raw chemicals in the petrochemical industry, and demand for these light olefins continues to increase year by year. Most light olefins are produced by steam cracking of naphtha, but the output composition is uncontrollable and propylene and butenes are present as by-products. In addition, steam cracking of naphtha occurs at high temperature so consumes a large amount of energy. Therefore, processes to obtain controlled production of light olefins under mild reaction conditions are very desirable.

Zeolites are crystalline aluminosilicates with three-dimensionally connected framework structures and have important properties such as strong acidity, high surface area, and regular pores with sizes close to the molecular size of hydrocarbons. In addition, zeolites are stable under high temperature conditions, so are widely used in industrial processes.

Production of light olefins from various sources such as naphtha[1)~10)], methanol[11)~16)], ethanol[17)] and acetone[18)~20)] over zeolite catalysts has been investigated extensively, and the reaction mechanisms over zeolite have also been evaluated[21)~30)]. Light olefins are intermediate products of the reaction, so suppression of consecutive reactions forming aromatics and coke from light olefins is required for selective production. Furthermore, the pore size of zeolites is close to the molecular size of light olefins and aromatics, so the reaction rates on acid sites and diffusion velocities of molecules inside the pores, which are related to the residence time of molecules inside the pores, strongly affect the progress of such undesirable reactions. Previously, silylated[18),19)] or alkali-metal ion exchanged[20)] zeolites were prepared intended to weaken the acid sites, which succeeded in producing isobutylene selectively from acetone. Isomorphous substitution of Al by other trivalent elements (*e.g.*, B, Ga, Fe and Zr) in the zeolite framework[31),32)], such as LTA, MFI, MTW and MOR, to form metallosilicates can modify the acidity of zeolites. For example, the methanol to olefins reaction over ferrisilicate with MFI-type zeolite structure showed low selectivity for aromatics[33),34)].

In the catalytic reaction over zeolite, the feedstock must diffuse inside the zeolite pores from the bulk fluid because the active sites are located on the surfaces of the zeolite pores. The product molecules formed on

DOI: doi.org/10.1627/jpi.60.277
* To whom correspondence should be addressed.
* E-mail: nakasaka@eng.hokudai.ac.jp

the active sites must then diffuse out of the zeolite pores to the bulk fluid. The diffusion rate is expressed as D_{eff}/R^2, where D_{eff} is the effective diffusivity and R is diffusion length. Therefore, shortening the diffusion length, *e.g.*, by decreasing the crystal size of the zeolite, will result in shorter residence time. Previously, nano-crystalline zeolites have been hydrothermally synthesized using water/surfactant/organic mixtures (emulsion method)[35),36)]. Kinetic analysis of *n*-hexane cracking over nano-sized MFI-type zeolite showed that the cracking proceeded under reaction control conditions, indicating that the effect of *n*-hexane diffusivity within the zeolite pores on the reaction rate was small[9)]. In addition, *n*-hexane cracking over the nano-sized zeolites improved the catalytic activity and catalyst lifetime compared to conventional macro-sized zeolites[37)].

The present study describes the production of light olefins from acetone and methanol over metallosilicates[38)~40)]. Macro- and nano-sized ferrisilicates and aluminosilicates with MFI and MTW structures were prepared using conventional hydrothermal synthesis and the emulsion method. In addition, nano-sized ferroaluminosilicates with MFI and MTW structures, containing both Fe and Al atoms in the zeolite framework, were also synthesized. These catalysts were evaluated for the conversion of acetone and/or methanol to olefins and the effects of crystal size and differences in strong acid site strength on the activity and light olefin selectivity are discussed based on the proposed reaction mechanisms.

2. Preparation and Characterization of Metallosilicates

2. 1. Preparation of Metallosilicates

Macro-sized and nano-sized metallosilicates with MFI-type zeolite structures were prepared by conventional hydrothermal synthesis or hydrothermal synthesis using a water/non-ionic surfactant/organic solvent mixture[35),36)]. Tetraethyl orthosilicate, alumino isopropoxide and iron(III) nitrate enneahydrate were used as the Si source, Al source and Fe source, respectively. Tetrapropyl ammonium hydroxide (TPAOH) and sodium chloride were used as the organic structure directing agent (OSDA) and alkali source, respectively. For the synthesis of macro-sized MFI-type ferrisilicate (macro-Fe-MFI), an aqueous solution containing the Si source, Fe source and OSDA was poured into a Teflon-sealed stainless steel bottle and hydrothermally treated at 423 K for 72 h. For the synthesis of nano-sized MFI-type zeolite (nano-Al-MFI), ferrisilicate (nano-Fe-MFI), and ferroaluminosilicate with MFI-type zeolite structure [nano-(Fe,Al)-MFI], an aqueous solution containing the Si, Al and/or Fe source and OSDA was added to a polyoxyethylene-(15)-oleyl ether/cyclohexane solution with surfactant concentration of 0.5 mol/L. The Si/T (T: Fe and/or Al) ratio in the aqueous solution was 100. The molar ratio of the aqueous solution to surfactant in the solution was 11. The resulting solution was then hydrothermally treated in a Teflon-sealed stainless steel bottle at 423 K for 72 h.

Synthesis of metallosilicates with MTW-type zeolite structures used a conventional hydrothermal method. Colloidal silica, sodium aluminate and iron(III) nitrate enneahydrate were used as the Si source, Al source and Fe source, respectively. Tetraethylammonium bromide (TEABr; for nano-sized zeolite) or triethylmethylammonium chloride (MTEACl; for macro-sized zeolite) were used as the OSDAs. An aqueous solution containing the Si, Al and/or Fe source and OSDA was placed in a Teflon-sealed stainless steel bottle and hydrothermally treated at 423 K for 144 h. The Si/T ratio (T: Fe and/or Al) in the solution was 100. The obtained products were washed well with distilled water and 2-propanol, and dried overnight at 383 K. The products were then calcined in a muffle furnace at 823 K for 12 h in air.

The crystallinity and morphology of the products were analyzed by X-ray diffraction (XRD; JDX-8020, JEOL Ltd. or UltimaIV, Rigaku Corp.) and field-emission scanning electron microscopy (FE-SEM; JSM-6500F, JEOL), respectively. The surface area and micropore volume of the product were calculated via the BET and t-plot method from nitrogen adsorption isotherms (Belsorp-mini, MicrotracBEL Corp.). The compositions of the product were analyzed by X-ray fluorescence spectrometer (XRF, Rigaku Supermini 200). The acidity of the product was evaluated from its *ac*-temperature-programmed desorption of ammonia (NH_3-TPD) profile[41)]. In addition, UV-vis diffuse reflectance spectra of the products in the wavelength range from 200 to 700 nm were measured.

2. 2. Characterization of Metallosilicate

XRD patterns of prepared samples of the metallosilicates with MFI-type zeolite structures are shown in **Fig. 1(a)**. All samples indicated peaks corresponding to the MFI-type zeolite phase, confirming the formation of ferrisilicate and ferroaluminosilicate with MFI-type zeolite structures. **Figure 2** shows FE-SEM images of the obtained samples. **Figure 2(a)** shows macro-Fe-MFI with coffin shape with a crystal size of approximately 1.2 μm. On the other hand, metallosilicates [nano-Al-MFI, nano-Fe-MFI and nano-(Fe,Al)-MFI] prepared by the emulsion method formed spherical shapes of approximately 100 nm. As shown in **Table 1**, the micropore volumes and BET surface areas estimated from nitrogen adsorption isotherms of each sample were approximately 0.17 $cm^3\,g^{-1}$, and in the range of 350-400 $m^2\,g^{-1}$, respectively, indicating that well-crystallized metallosilicates with MFI-type zeolite structures could be obtained regardless of the atomic species in the framework and crystal size.

To confirm incorporation of Fe atoms into the zeolite framework, UV-vis spectra of the prepared metallosilicate with MFI-type zeolite structure were measured as shown in **Fig. 3**. For comparison, a UV-vis spectrum of the physically mixed SiO_2 and Fe_2O_3 was measured and a broad spectrum was observed. The bands between 200 nm and 300 nm indicate that Fe species existed as isolated Fe^{3+}, either tetrahedrally coordinated in the zeolite framework or with higher coordination. Bands between 300 nm and 450 nm and bands above 450 nm are characteristic of octahedral Fe^{3+} ions in small oligonuclear $Fe_x^{3+}O_y$ complexes and Fe^{3+} ions in large aggregated iron oxides, respectively[42]. The UV-vis spectra of Fe containing MFI-type zeolites showed peaks below 300 nm and no peaks above 450 nm, indicating the presence of small oligonuclear $Fe_x^{3+}O_y$ complexes and/or iron oxide was lower than the detection limit, and Fe^{3+} species in the obtained samples were well isolated.

To evaluate the isomorphous substitution of Fe atoms in the zeolite framework, the number of acid sites in the obtained zeolites was measured by *ac*-NH_3-TPD. **Figure 4** shows *ac*-NH_3-TPD profiles of nano-Fe-MFI, nano-Al-MFI and nano-(Fe,Al)-MFI. Peaks below 550 K correspond to desorption of ammonia physically adsorbed on the zeolites. Peaks above 550 K are assigned to desorption of ammonia adsorbed on the strong acid site of zeolite. These samples showed ammonia desorption peaks above 550 K, indicating the presence of strong acid sites. Formation of strong acid sites is related to the presence of framework hetero-

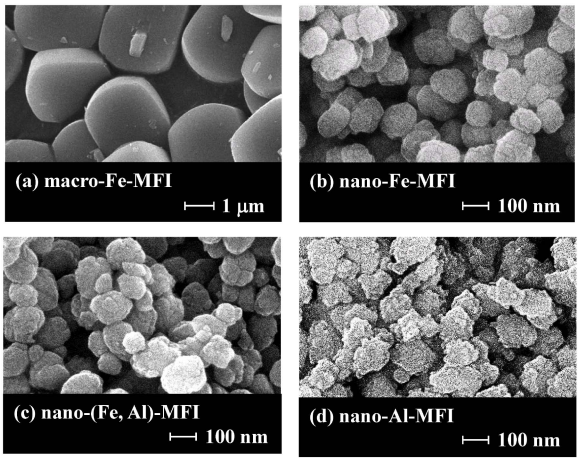

Fig. 2 FE-SEM Images of (a) Macro-Fe-MFI, (b) Nano-Fe-MFI, (c) Nano-(Fe,Al)-MFI and (d) Nano-Al-MFI Zeolites

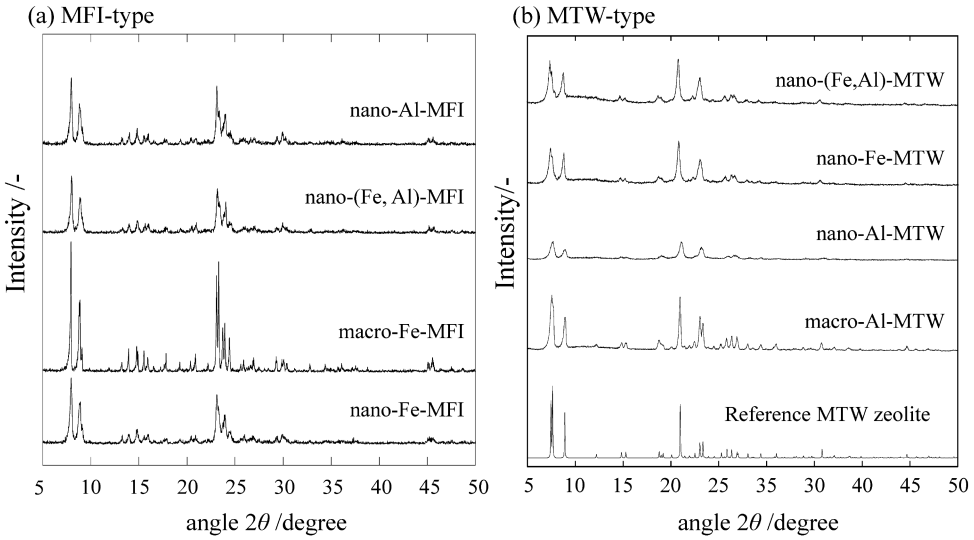

Fig. 1 XRD Patterns of Metallosilicates with MFI and MTW Structures

Table 1 Si/T Ratio, Micropore Volume and BET Surface Area of Zeolites

Sample	Si/T[a)] [-]	V_m [$m^3\ g^{-1}$]	S_{BET} [$m^2\ g^{-1}$]
macro-Fe-MFI	107	0.17	366
nano-Fe-MFI	102	0.18	385
nano-Al-MFI	105	0.17	395
nano-(Fe,Al)-MFI	99	0.17	350
nano-Fe-MTW	88	0.13	352
nano-Al-MTW	122	0.12	343
nano-(Fe,Al)-MTW	104	0.11	304

a) Si/T ratios are measured by XRF.

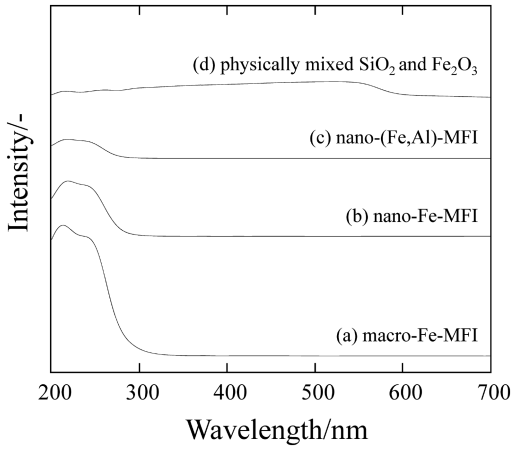

Fig. 3 UV-vis Spectra of Fe Containing Zeolites: (a) macro-Fe-MFI, (b) nano-Fe-MFI, (c) nano-(Fe,Al)-MFI, and (d) physically mixed SiO_2 and Fe_2O_3.

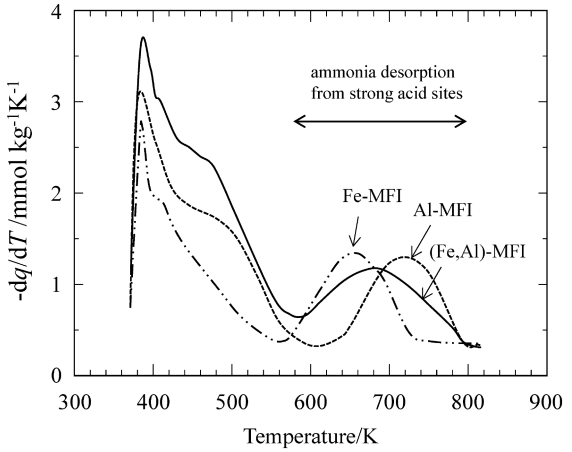

Fig. 4 *ac*-NH_3-TPD Profiles of Nano-Fe-MFI, Nano-Al-MFI and Nano-(Fe,Al)-MFI

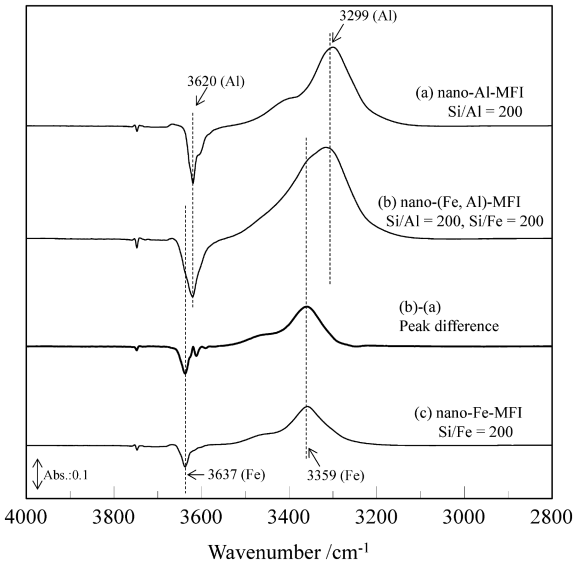

Fig. 5 IR Spectra of CO Adsorbed on the Zeolites: (a) nano-Al-MFI, (b) nano-(Fe,Al)-MFI and (c) nano-Fe-MFI

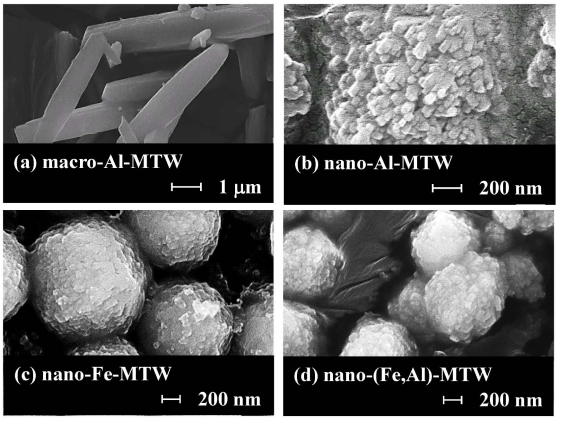

Fig. 6 FE-SEM Images of (a) Macro-Al-MTW, (b) Nano-Al-MTW, (c) Nano-Fe-MTW and (d) Nano-(Fe,Al)-MTW

atoms, so this observation confirms the isomorphous substitution of Fe in the MFI-type framework. Moreover, the number of acid sites in all samples was in the range from 0.16 to 0.17 mol kg^{-1}, which is almost the same value as calculated for an MFI-type zeolite with a Si/T ratio of 100.

The above results demonstrate that Fe atoms in the synthesis solution are well incorporated in the MFI-type framework. In addition, the ammonia desorption peak of Fe-MFI is lower than that of Al-MFI, indicating that the acid site strength of Fe-MFI is weaker than that of Al-MFI. Macro-Fe-MFI had almost the same NH_3-TPD profile as nano-Fe-MFI (data not shown). IR spectra of CO adsorbed on Fe-MFI, Al-MFI and (Fe, Al)-MFI were also measured (**Fig. 5**). The spectrum obtained by subtracting the spectrum of nano-Al-MFI (Si/Al = 200) from the spectrum of nano-(Fe,Al)-MFI was close to the spectrum of nano-Fe-MFI. Therefore, two types of Brønsted acid sites, derived from Fe and Al atoms in the framework, were formed in nano-(Fe,Al)-MFI[39].

XRD patterns of synthesized samples of metallosilicates with MTW-type zeolite structures were measured (**Fig. 1(b)**). Peaks corresponding to MTW-type zeolite structures were observed regardless of the OSDA and T-site atomic species. FE-SEM photographs of these samples are shown in **Fig. 6**. MTW-type zeolites with different crystal sizes were obtained using different OSDAs. Al-MTW, Fe-MTW and (Fe,Al)-MTW synthesized using TEABr formed nano-sized crystal aggregated to form secondary particles, regardless of T site atom species. In contrast, Al-MTW synthesized using MTEACl formed macro-sized crystals. UV-vis spectra and *ac*-NH_3-TPD profiles of these samples confirmed that the majority of Fe^{3+} species in the synthesized samples were well isolated and the Fe atoms were

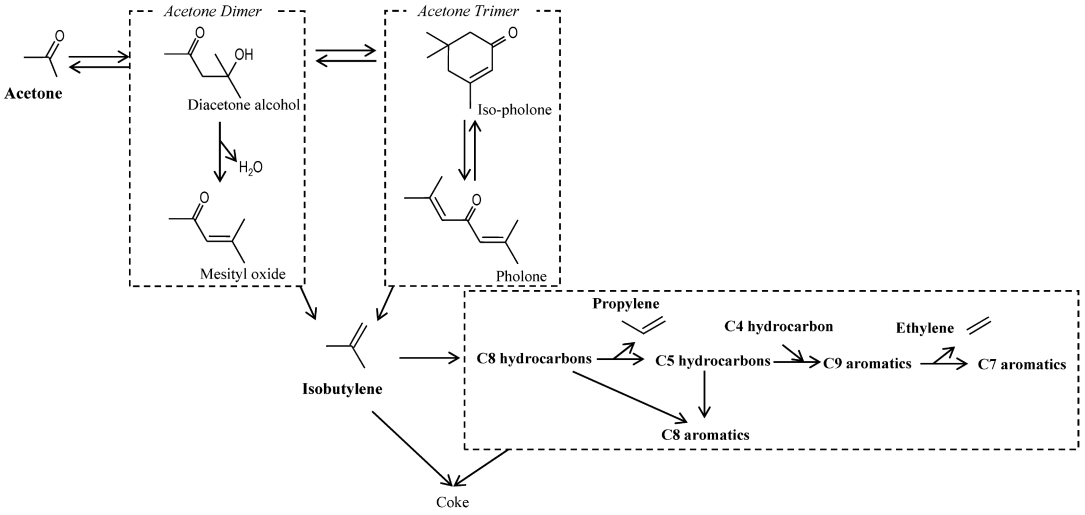

Fig. 7 Proposed Acetone to Olefins Reaction Pathway over Solid-acid Catalyst

incorporated into the MTW-type zeolite framework.

3. Light Olefins Synthesis from Acetone

In addition to ethylene and propylene, butenes are important raw materials in the petrochemical industry as a feedstock for the production of methacrylate, butyl rubber and ethyl *t*-butyl ether. Isobutylene can also be produced from acetone over a solid-acid catalyst. In the commercial cumene process, an equimolar amount of acetone is produced as a by-product. Moreover, acetone can be obtained from biomass-derived tar over an iron oxide catalyst[43),44)]. Accordingly, the acetone to olefins reaction over an acid catalyst is a candidate for selective production of isobutylene.

A proposed reaction pathway from acetone to light olefins[28)~30)] is shown in **Fig. 7**. First, acetone dimer and trimer formed by aldol condensation of acetone are decomposed to form isobutylene. Isobutylene then reacts with itself to form C8 hydrocarbons followed by formation of C8 aromatics and propylene. Finally, coke is formed on the zeolite[18)]. Therefore, as the olefins are intermediate products in the consecutive reactions, suppression of aromatics and coke formation from light olefins is essential for selective production of light olefins.

The acetone to olefins reaction over nano-Fe-MFI and nano-Al-MFI was carried out using a fixed bed type reactor at a temperature of 723 K under atmospheric pressure. The *W*/*F* ratio (*W*: catalyst weight in the reactor [g]; *F*: acetone flow rate [g h^{-1}]) was adjusted in the range from 0.1 to 0.5 h. Nitrogen was fed into the reactor as a carrier gas. The composition of the exit gas was analyzed using an on-line gas chromatograph (GC-2014, Shimadzu Corp.) with a Porapak-Q column and thermal conductivity detector (TCD), and with a Gaskuropack 54 and hydrogen-flame ionization detector (FID). The amount of coke deposited on the catalyst during the reaction was measured by thermogravimetry (TGA-50, Shimadzu). Prior to the reaction, catalysts were activated under air flow at 823 K for 1 h to exchange the active sites from the NH_4^+ form to the H^+ form.

The acetone conversion and product selectivity over nano-Fe-MFI and nano-Al-MFI at 20 min and 260 min are shown in **Table 2**. The acid site strengths of Fe-MFI and Al-MFI were different, so the catalyst loading in the reactor was adjusted to obtain the same initial conversion (approximately 70 C-mol%). As shown in **Table 2**, nano-Fe-MFI showed higher selectivity for light olefins and lower selectivity for aromatics compared to nano-Al-MFI. Nano-Fe-MFI exhibited very high isobutylene composition above 90 C-mol% and ethylene and propylene composition were both lower than 10 C-mol%. In contrast, nano-Al-MFI showed much higher ethylene and propylene compositions than nano-Fe-MFI. In addition, the amount of coke formed on nano-Fe-MFI during the reaction was 0.6 wt%, which was lower than that on nano-Al-MFI (3.2 wt%). These results indicate that the weak acid sites of Fe-MFI effectively suppressed the consecutive reactions from isobutylene to ethylene, propylene and aromatics, leading to high isobutylene selectivity and low coke formation.

The diffusion length of molecules inside zeolite pores affects the progress of the consecutive reactions, so macro-Fe-MFI was also used to catalyze the acetone to olefins reaction. Acetone conversion and product selectivity over macro- and nano-Fe-MFI zeolites are shown in **Table 2**. Although acetone conversion over macro-Fe-MFI decreased to 30 C-mol% after 620 min, nano-Fe-MFI maintained acetone conversion at 45 C-mol%. The selectivity for aromatics of nano-Fe-MFI during the reaction was lower compared to macro-

Table 2 Acetone Conversion and Product Selectivity over Nano-Al-MFI, Nano-Fe-MFI and Macro-Fe-MFI

	nano-Al-MFI		nano-Fe-MFI		macro-Fe-MFI	
Reaction time [min]	20	260	20	260	20	260
Conversion [C-mol%]	67.9	47.8	67.6	53.9	69.7	48.4
Selectivity [C-mol%]						
methane	0.1	0.4	3.9	3.8	4.8	3.9
light olefin	47.4	57.7	80.2	85.8	73.8	83.6
paraffin	0.9	0.8	0.5	0.3	0.5	0.2
aromatics	39.4	22.6	6.9	4.1	11.6	7.9
others	12.2	18.6	8.6	6.0	9.2	4.4
Light olefins composition [C-mol%]						
ethylene	9.8	4.7	0.7	0.4	1.5	1.0
propylene	30.7	26.5	9.3	6.7	9.9	4.9
isobutylene	59.5	68.8	90.0	92.9	88.6	94.1

Fe-MFI. In addition, coke loadings on macro- and nano-Fe-MFI after the reaction were 4.9 wt% and 1.0 wt%, respectively. The residence times of reactant and product molecules inside the zeolite pore decreased with smaller crystal size of the zeolite, so consecutive reactions forming aromatics and coke, which cause deactivation of the zeolite, were suppressed by nano-Fe-MFI.

Although coke formation could be suppressed by weakening the acid site strength and reducing the crystal size of the ferrisilicate with MFI-type zeolite structure, formation of a small amount of coke during the reaction is unavoidable. In general, coke combustion is carried out to regenerate coked catalyst. During the regeneration, steam is produced due to oxygenation of the hydrogen in coke and the catalyst bed temperature increases because the reaction is exothermic. Treatment of the zeolite under hydrothermal atmosphere at high temperature causes dealumination of the zeolite framework leading to deactivation of the zeolite[45),46)]. Therefore, the durability of Fe atoms in the Fe-MFI was investigated. **Figure 8** shows the change in acetone conversion over nano-Fe-MFI after three reaction/regeneration cycles. Acetone conversion and catalyst regeneration were carried out at 723 K and 823 K, respectively. Compared to the first reaction, acetone conversion in the second and third reactions was slightly lower. However, the changes in acetone conversion and selectivity of products during the third reaction were close to those during the second reaction, indicating that Fe atoms remained in the zeolite framework after regeneration and the Fe atoms in the framework were stable during the regeneration process.

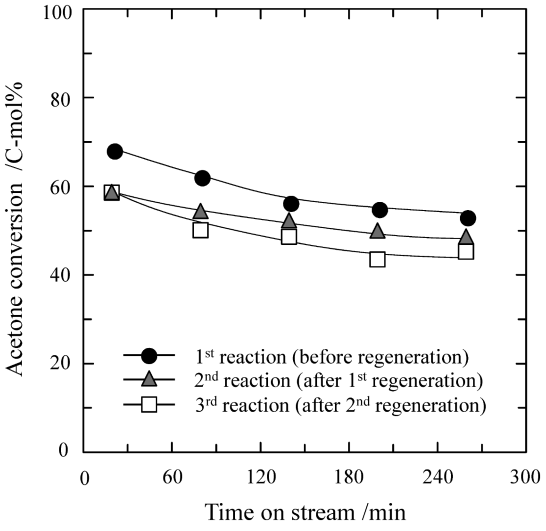

Reaction temperature: 723 K, *W/F* ratio: 0.5 kg-cat./(kg-acetone h^{-1}).

Fig. 8 Changes in Acetone Conversion with Time on Stream over Nano-Fe-MFI before/after Regeneration

4. Synthesis of Light Olefins from Methanol

The methanol to olefins reaction produces light olefins selectively, and can be catalyzed by various types of zeolites and zeotype materials. Zeolites and zeotype materials with small pores, such as SAPO-34 and ZSM-5, have higher selectivity for light olefins[14)~16)]. Recently, CON-type aluminosilicate possessing three dimensional channels with 12-, 12-, and 10-ring pores showed high selectivity for propylene in the methanol to olefins reaction[13)].

Reaction mechanisms of the methanol to olefins include a hydrocarbon pool reaction mechanism[21),22)] and a dual-cycle mechanism (**Fig. 9**)[23)~26)]. The dual-cycle mechanism involves: (a) an alkene methylation/cracking cycle producing propylene, butenes and higher alkenes, and (b) an aromatic-based cycle producing ethylene and aromatics by cyclization of the higher alkenes formed in the alkene methylation/cracking cycle.

4. 1. Methanol to Olefins Reaction over Metallosilicates with MFI Structures

The methanol to olefins reaction over Fe-MFI with different crystal sizes was carried out at a reaction temperature of 673 K. **Figure 10** shows the effect of

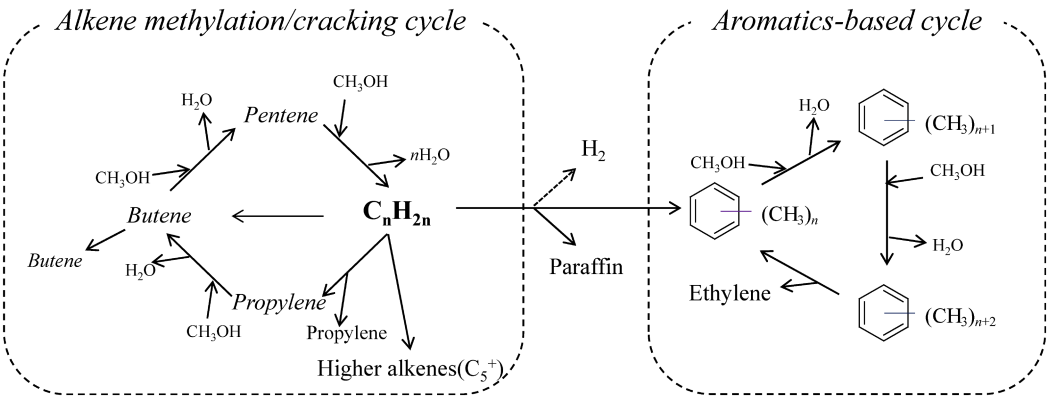

Fig. 9 Proposed Methanol to Olefins Reaction Mechanism over MFI-type Zeolite by Olsbye *et al.*[26)]

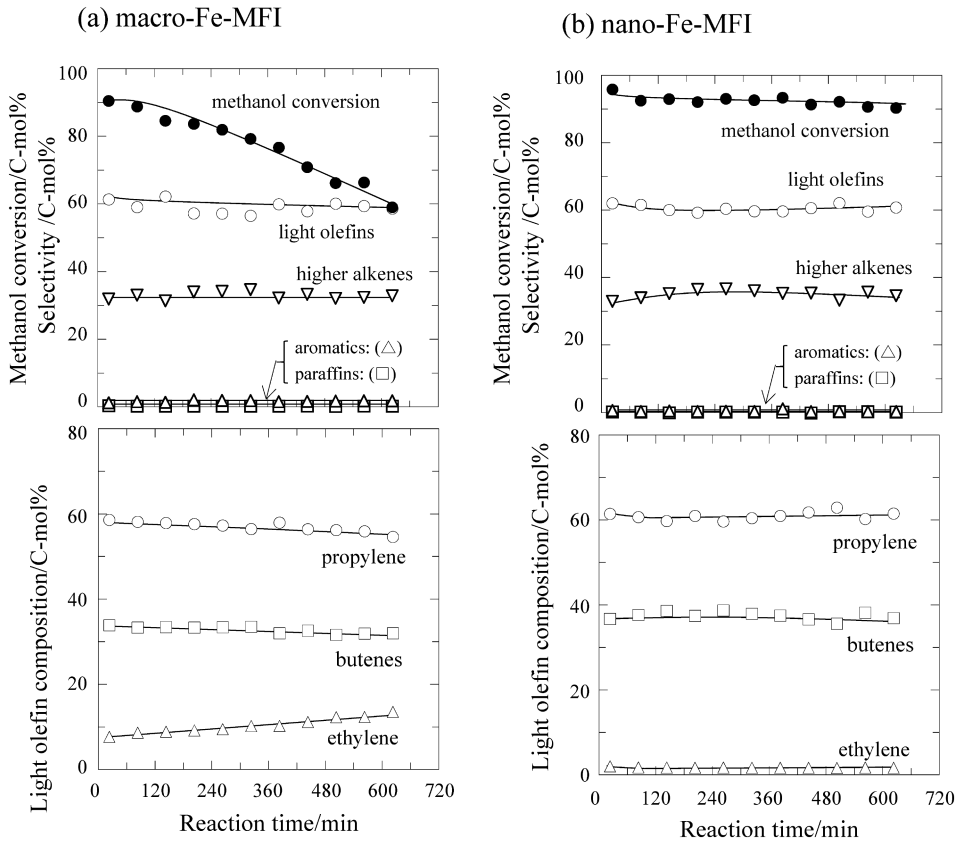

Fig. 10 Changes in Methanol Conversion, Product Selectivity and Light Olefin Composition with Time on Stream over Fe-MFI with Different Crystal Sizes at a Reaction Temperature of 673 K with a *W/F* Ratio of 0.2 h

crystal size of Fe-MFI on methanol conversion and product selectivity. Nano-Fe-MFI showed consistent methanol conversion above 90 C-mol% and stable product selectivity. In contrast, macro-Fe-MFI showed gradually decreasing methanol conversion to 60 C-mol% after 620 min due to deactivation by coke formation. The amounts of coke formed on macro- and nano-Fe-MFI after the reaction were 5.1 wt% and 1.1 wt%, respectively. Macro-Fe-MFI yielded higher ethylene composition compared to nano-Fe-MFI. Based on the dual-cycle mechanism (**Fig. 9**), ethylene production occurred in the second aromatics-based cycle. Larger crystal size results in longer residence time of the product inside the zeolite pore. This longer residence time allowed progress of the consecutive reactions forming aromatics and coke. Therefore, smaller crystal size is essential for suppression of the second aromatics-based cycle. In the methanol to olefins

Table 3 Methanol Conversion and Product Selectivity over Nano-Fe-MFI, Nano-Al-MFI, Nano-(Fe,Al)-MFI and Blended Sample at 260 min (reaction temperature: 723 K)

		nano-Fe-MFI $W/F = 0.2$ h	nano-Al-MFI $W/F = 0.05$ h	nano-(Fe,Al)-MFI $W/F = 0.1$ h	Blended sample $W/F = 0.1$ h
Conversion	[C-mol%]	98.6	98.2	98.8	99.7
Selectivity	[C-mol%]				
methane		2.3	0.4	0.6	0.8
ethylene		2.0	7.8	3.9	8.2
propylene		33.5	32.8	44.1	38.4
butenes		19.9	13.5	20.2	17.1
paraffin		0.2	8.7	1.4	6.3
higher alkenes (C5+)		37.6	25.9	26.0	21.0
aromatics		3.3	7.2	2.7	5.9
others		1.3	3.7	1.0	2.3
P/E ratio	[-]	17.1	4.2	11.2	4.7

reaction over Fe-MFI, large amounts of higher alkenes were produced in the first alkene methylation/cracking cycle. Catalytic cracking of the higher alkenes is required to increase propylene yield, so strong acid sites were introduced into the Fe-MFI framework by preparing (Fe,Al)-MFI.

Table 3 shows the methanol conversion, product selectivity and propylene to ethylene ratio (P/E) at 260 min over nano-sized Fe-MFI, Al-MFI and (Fe,Al)-MFI. To obtain approximately the same initial conversion, the *W*/*F* ratio was adjusted for each catalyst. Nano-(Fe,Al)-MFI showed increased selectivity for propylene and decreased selectivity for higher alkenes and aromatics compared to Fe-MFI, indicating that nano-(Fe,Al)-MFI enhanced the cracking of higher alkenes produced in the alkene methylation/cracking cycle by suppressing the second aromatics-based cycle. Moreover, nano-(Fe,Al)-MFI had higher selectivity for propylene than nano-Al-MFI, which showed the highest aromatics selectivity.

To confirm that the advantageous characteristics of nano-(Fe,Al)-MFI are derived from incorporation of Fe and Al in the same structure, a physically blended sample, containing 50 wt% of Fe-MFI and 50 wt% of Al-MFI, was prepared and used for the methanol to olefins reaction under the same conditions as nano-(Fe,Al)-MFI. The physically blended sample had lower selectivity for higher alkenes, and higher selectivity for ethylene and aromatics compared with nano-(Fe,Al)-MFI, indicating that higher alkenes aromatization was enhanced and ethylene and aromatics were produced in the second cycle. Moreover, the product selectivity over the physically blended sample was closer to that over nano-Al-MFI. Clearly, the progress of the consecutive reactions depends on the acidity of the zeolite. The acidity of Al-MFI is stronger than that of Fe-MFI, so the physically blended sample showed similar catalytic performance to nano-Al-MFI. In addition, the methanol to olefins reaction over nano-(Fe,Al)-MFI with different *W*/*F* ratios (0.05, 0.1 and 0.15 h) showed selectivity for propylene reached 48 C-mol% with the P/E ratio above 10 and the *W*/*F* ratio of 0.15 h.

4. 2. Methanol to Olefins Reaction over Metallosilicate with MTW Structures

The pores of MFI-type zeolites provide adequate volume for the formation of key reactive intermediates in the methanol to olefins reaction[47], but also provide sufficient volume for cyclization of higher alkenes produced in the alkene methylation/cracking cycle, because the size of the channel intersection in MFI-type zeolites is nearly 0.9 nm[48]. MTW-type zeolites containing one-dimensional 12-ring pores (0.56×0.6 nm) also provide adequate volume for the key intermediates, but the pores are smaller than the channel intersection in MFI-type zeolites. Therefore, cyclization of higher alkenes is expected to be suppressed using MTW-type zeolites. However, the methanol to olefins reaction over MTW-type zeolites has not been extensively studied[47),49].

Al-MTW zeolites with different crystal sizes were used to catalyze the methanol to olefins reaction. The reaction was carried out at a reaction temperature of 723 K with a *W*/*F* ratio of 0.1 h. The change in methanol conversion with time over Al-MTW with different crystal sizes is shown in **Fig. 11**. Methanol conversion drastically decreased with time over macro-Al-MTW, whereas methanol conversion and product selectivity were stable over nano-Al-MTW. The coke amount formed on macro-Al-MTW after the reaction was 5.9 wt%, which was much higher than that on nano-Al-MTW (0.9 wt%). **Figure 12** shows nitrogen adsorption isotherms of these MTW-type zeolites before and after the reaction. The nitrogen adsorption isotherm of nano-Al-MTW after the reaction was almost the same as that before the reaction. In contrast, macro-Al-MTW after the reaction showed very little nitrogen adsorption, indicating that the zeolite pores were plugged by coke formation. MTW-type zeolites possess a one-dimensional pore structure, so aromatics and coke formation leads to plugging of the pores followed by fast deactivation. Therefore, smaller

crystal size of the zeolite with one-dimensional pores achieves stable activity due to the larger external surface area and smaller diffusion resistance of molecules.

To investigate the effect of the acid site strength of MTW-type zeolites and zeolite structures, nano-Fe-MTW and nano-Al-MFI were also used to catalyze the methanol to olefins reaction at 723 K with a *W/F* ratio of 0.1 h. Methanol conversion and product selectivity at 20 min are shown in **Table 4**. Nano-Al-MFI showed higher selectivity for aromatics and ethylene compared to other catalysts. The channel intersections of MFI-type zeolites are large enough for the cyclization reaction, so that the aromatics-based cycle became more important. In contrast, MTW-type zeolites with one-dimensional pore structures do not provide such space, which suppresses cyclization inside the pores.

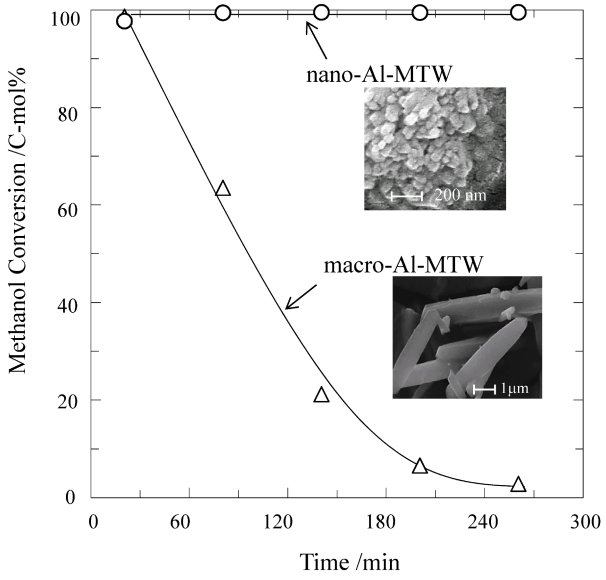

Fig. 11 Changes in Methanol Conversion with Time on Stream over Macro- and Nano-Al-MTW

Nano-Fe-MTW showed lower methanol conversion and higher alkene (C5+) selectivity than nano-Al-MTW due to the weaker acidity of nano-Fe-MTW. On the other hand, although nano-Al-MTW had higher selectivity for propylene, some ethylene, aromatics and paraffins formation was also confirmed due to the action of the aromatics-based cycle. To decrease the contribution of the aromatics-based cycle while maintaining the C5+ cracking activity, (Fe,Al)-MTW containing both strong and weak acid sites was used for the reaction at 723 K with a *W/F* ratio of 0.2 h.

Propylene and butenes selectivity over nano-(Fe,Al)-MTW was higher compared to nano-Al-MTW, with the total yield of propylene and butenes above 70 C-mol%. Moreover, nano-(Fe,Al)-MTW showed lower selectivity for ethylene, aromatics and C5+ compared to both nano-Al-MTW and nano-Fe-MTW, indicating that introduction of weak acid sites to Al-MTW suppressed the action of the aromatic-based cycle while maintaining the C5+ cracking activity. In addition, methanol conversion and product selectivity over nano-(Fe,Al)-MTW were maintained at almost the same values after 260 min and no deactivation was observed, indicating that nano-sized metallosilicate with MTW-type zeolite structure containing both Al and Fe atoms in the framework was effective for the production of propylene and butenes from methanol.

5. Conclusion

Ferrisilicates with different crystal sizes were used to catalyze the acetone to olefins and methanol to olefins reactions. Nano-sized Fe-MFI had stable and longer lifetimes in both reactions due to suppression of side reactions from light olefins to aromatics and coke by decreasing the diffusion length of the feedstock and product molecules. The acid site strength of MFI-type zeolites strongly affected the progress of these consecu-

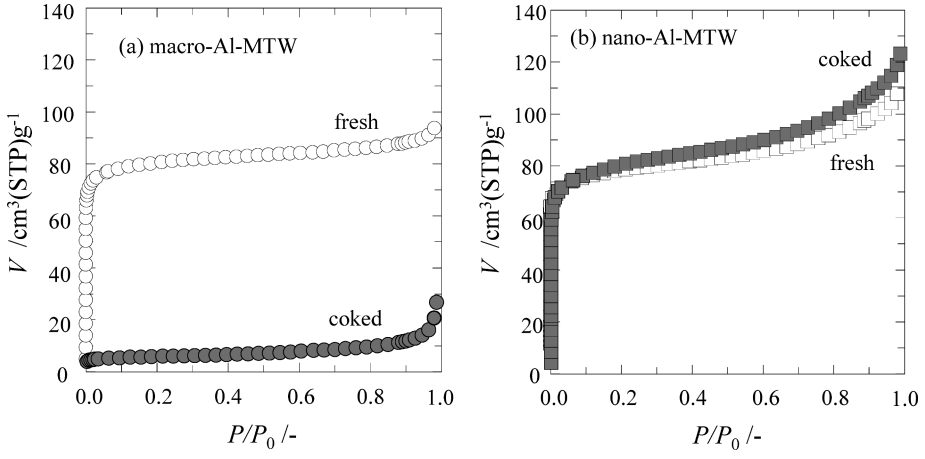

Fig. 12 Nitrogen Adsorption Isotherms of (a) Macro-Al-MTW and (b) Nano-Al-MTW before/after the Methanol to Olefins Reaction

Table 4 Methanol Conversion, Product Selectivity and P/E Ratio over Nano-Fe-MTW, Nano-Al-MTW, Nano-(Fe,Al)-MTW, and Nano-Al-MFI at 20 min (temperature: 723 K)

		nano-Fe-MTW $W/F = 0.1$ h	nano-Al-MTW $W/F = 0.1$ h	nano-(Fe,Al)-MTW $W/F = 0.2$ h	nano-Al-MFI $W/F = 0.1$ h
Conversion	[C-mol%]	72.5	97.8	98.4	99.9
Selectivity	[C-mol%]				
methane		7.3	0.3	1.8	0.4
ethylene		4.2	4.4	3.1	8.4
propylene		26.4	49.9	52.4	41.3
butenes		17.9	18.1	20.2	20.6
paraffin		0.4	3.8	1.9	3.5
higher alkene (C5+)		34.2	19.3	18.4	19.9
aromatics		3.8	2.7	1.1	3.9
others		5.7	1.6	1.1	1.9
P/E ratio	[-]	6.3	11.5	16.8	4.9

tive reactions, and nano-Fe-MFI achieved selective production of isobutylene from acetone. Although nano-Fe-MFI could suppress consecutive reactions forming aromatics and coke in the methanol to olefins reaction, the weaker acid sites of Fe-MFI did not catalyze higher alkene cracking. Nano-(Fe,Al)-MFI containing both Fe and Al atoms in the MFI framework achieved higher selectivity for propylene of 48 C-mol% and higher P/E ratio of 11.5 at 723 K with the *W/F* ratio of 0.15 h.

Nano-(Fe,Al)-MTW showed higher selectivity for propylene and butenes in the methanol to olefins reaction and suppressed formation of aromatics and ethylene which are formed by cyclization of higher alkenes. The one-dimensional pore structure and presence of two types of Brønsted acid sites, derived from Fe and Al atoms in the framework, effectively combined to result in the high yields of propylene and butenes (above 70 C-mol%) from methanol.

Acknowledgment

We would like to thank Dr. T. Yokoi at Tokyo Institute of Technology for measuring IR spectra of CO adsorbed on zeolites.

References

1) Corma, A., Mengual, J., Miguel, P. J., *Appl. Catal. A: General*, **421**, 121 (2012).
2) Kissin, Y. V., *J. Catal.*, **163**, 50 (1996).
3) Bhan, A., Gounder, R., Macht, J., Iglesia, E., *J. Catal.*, **253**, 221 (2008).
4) Inagaki, S., Takechi, K., Kubota, Y., *Chem. Commun.*, **46**, 2662 (2010).
5) Mochizuki, H., Yokoi, T., Imai, H., Watanabe, R., Namba, S., Kondo, J. N., Tatsumi, T., *Micropor. Mesopor. Mater.*, **145**, 165 (2011).
6) Kubo, K., Iida, H., Namba, S., Igarashi, A., *Micropor. Mesopor. Mater.*, **149**, 126 (2012).
7) Yamaguchi, A., Jin, D., Ikeda, T., Sato, K., Hiyoshi, N., Hanaoka, T., Mizukami, F., Shirai, M., *Fuel Proc. Technol.*, **126**, 343 (2014).
8) Urata, K., Furukawa, S., Komatsu, T., *Appl. Catal. A: General*, **475**, 335 (2014).
9) Nakasaka, Y., Okamura, T., Konno, H., Tago, T., Masuda, T., *Micropor. Mesopor. Mater.*, **182**, 244 (2013).
10) Corma, A., Mengual, J., Miguel, P. J., *Appl. Catal. A: General*, **460-461**, 106 (2013).
11) Kumita, Y., Gascon, J., Stavitski, E., Stavitski, E., Moulijn, J. A., Kapteijn, F., *Appl. Catal. A: General*, **391**, 234 (2011).
12) Chen, J. Q., Bozzano, A., Glover, B., Fuglerud, T., Kvisle, S., *Catal. Today*, **106**, 103 (2005).
13) Yoshioka, M., Yokoi, T., Tatsumi, T., *ACS Catal.*, **5**, 4268 (2015).
14) Park, J. W., Lee, J. Y., Kim, K. S., Hong, S. B., Seo, G., *Appl. Catal. A: General*, **339**, 36 (2008).
15) Firoozi, M., Haghalha, M., Asadi, M., *Catal. Commun.*, **10**, 1582 (2009).
16) Mei, C., Wen, P., Liu, Z., Liu, H., Wang, Y., Yang, W., Xie, Z., Hua, W., Gao, Z., *J. Catal.*, **258**, 243 (2008).
17) Goto, D., Harada, Y., Furumoto, Y., Takahashi, A., Fujitani, T., Oumi, Y., Sadakane, M., Sano, T., *Appl. Catal. A: General*, **383**, 89 (2010).
18) Tago, T., Konno, H., Sakamoto, M., Nakasaka, Y., Masuda, T., *Appl. Catal. A: General*, **403**, 183 (2011).
19) Konno, H., Tago, T., Nakasaka, Y., Watanabe, G., Masuda, T., *Appl. Catal. A: General*, **475**, 127 (2014).
20) Tago, T., Konno, H., Ikeda, S., Yamazaki, S., Ninomiya, W., Nakasaka, Y., Masuda, T., *Catal. Today*, **164**, 158 (2011).
21) Dahl, I. M., Kolboe, S., *J. Catal.*, **149**, 458 (1994).
22) Dahl, I. M., Kolboe, S., *J. Catal.*, **161**, 304 (1996).
23) Svelle, S., Joensen, F., Nerlov, J., Olsbye, U., Lillerud, K. P., Kolboe, S., Bjørgen, M., *J. Am. Chem. Soc.*, **128**, 14770 (2006).
24) Bjørgen, M., Svelle, S., Joensen, F., Nerlov, J., Kolboe, S., Bonino, F., Palumbo, L., Bordiga, S., Olsbye, U., *J. Catal.*, **248**, 195 (2007).
25) Bjørgen, M., Lillerud, K. P., Olsbye, U., Svelle, S., *Stud. Surf. Sci. Catal.*, **167**, 463 (2007).
26) Bjørgen, M., Joensen, F., Lillerud, K. P., Olsbye, U., Svelle, S., *Catal. Today*, **142**, 90 (2009).
27) McAllister, S. H., Bailey, W. A., Bouton, C. M., *J. Am. Chem. Soc.*, **62**, 3210 (1940).
28) Cejka, J., Kubelkova, L., Jiru, P., *Collect. Czech. Chem. Commun.*, **54**, 2998 (1989).
29) Kubelkova, L., Cejka, J., Novakova, J., *Zeolites*, **11**, 48 (1991).
30) Panov, A. G., Fripiat, J. J., *J. Catal.*, **178**, 188 (1998).
31) Asensi, M. A., Corma, A., Martínez, A., Derewinski, M., Krysciak, J., Tamhankar, S. S., *Appl. Catal. A: General*, **174**, 163 (1998).
32) Gabelica, Z., Valange, S., *Micropor. Mesopor. Mater.*, **30**, 57 (1999).

33) Inui, T., Matsuda, T., Yamase, O., Nagata, H., Fukuda, K., Ukawa, T., Miyamoto, A., *J. Catal.*, **98**, 491 (1986).
34) Ahmed, S., *J. Porous. Mater.*, **19**, 111 (2012).
35) Tago, T., Nishi, M., Kono, Y., Masuda, T., *Chem. Lett.*, **33**, 1040 (2004).
36) Iwakai, K., Tago, T., Konno, H., Nakasaka, Y., Masuda, T., *Micropor. Mesopor. Mater.*, **141**, 167 (2011).
37) Konno, H., Okamura, T., Kawahara, T., Nakasaka, Y., Tago, T., Masuda, T., *Chem. Eng. J*., **207**-**208**, 460 (2012).
38) Taniguchi, T., Nakasaka, Y., Yoneta, K., Tago, T., Masuda, T., *Micropor. Mesopor. Mater.*, **224**, 68 (2016).
39) Taniguchi, T., Yoneta, K., Nakaoka, S., Nakasaka, Y., Yokoi, T., Tago, T., Masuda, T., *Catal. Lett.*, **146**, 442 (2016).
40) Taniguchi, T., Nakasaka, Y., Yoneta, K., Tago, T., Masuda, T., *Catal. Lett.*, **146**, 666 (2016).
41) Masuda, T., Fujikata, Y., Mukai, S. R., Hashimoto, K., *Appl. Catal. A: General*, **165**, 57 (1997).
42) Perez-Ramírez, J., *J. Catal.*, **227**, 512 (2004).
43) Fumoto, E., Mizutani, Y., Tago, T., Masuda, T., *Appl. Catal. B: Environmental*, **68**, 154 (2006).
44) Funai, S., Satoh, Y., Satoh, Y., Tajima, K., Tago, T., Masuda, T., *Top. Catal.*, **53**, 654 (2010).
45) Sano, T., Yamashita, N., Iwami, Y., Takeda, K., Kawakami, Y., *Zeolites*, **16**, 258 (1996).
46) Sano, T., Ikeya, H., Kasuno, T., Wang, Z. B., Kawakami, Y., Soga, K., *Zeolites*, **19**, 80 (1997).
47) Wang, Q., Cui, Z. M., Cao, C. Y., Song, W. G., *J. Phys. Chem. C*, **115**, 24987 (2011).
48) Song, Y., Zhu, X., Xie, S., Wang, Q., Xu, L., *Catal. Lett.*, **97**, 31 (2004).
49) Salehirad, F., Anderson, M. W., *J. Chem. Soc., Faraday Trans.*, **94**, 1911 (1998).

……

要　　旨

MFI 型，MTW 型ゼオライト構造を有するメタロシリケートを用いた含酸素有機物からの低級オレフィン合成

中坂　佑太[†1)]，多湖　輝興[†2)]，増田　隆夫[†1)]

[†1)] 北海道大学大学院工学研究院応用化学部門，060-8628 札幌市北区北13条西8丁目
[†2)] 東京工業大学物質理工学院応用化学系，152-8552 東京都目黒区大岡山2-12-1

低級オレフィンは逐次反応の中間体生成物であるため，ゼオライト触媒を用いた選択合成において逐次反応の制御が必須である。ゼオライトを触媒に用いる際，ゼオライト結晶内における反応原料，反応生成物の拡散抵抗およびゼオライト酸点の強度が触媒活性や生成物選択性に強く影響を及ぼす。本稿では，粒径の異なる MFI，MTW 型の構造を有するフェリシリケートおよびフェロアルミノシリケートの合成と，含酸素有機物であるアセトン，メタノールからの低級オレフィン合成について解説する。アセトンおよびメタノールからの低級オレフィン合成において，MFI 型構造を有するフェリシリケートナノ結晶はマクロ結晶に比べ安定な触媒活性を示した。さらに，両反応に対し骨格中に Fe を有するメタロシリケートは芳香族やコーク生成の抑制によりアルミノシリケートに比べ高い低級オレフィン選択性を示した。メタノールからの低級オレフィン合成において，ゼオライト骨格中の Fe および Al に由来する二種類のブレンステッド酸点を有するフェロアルミノシリケートが低級オレフィン合成に有効であった。

……